The Goddard Coastal Wave Model. Part I: Numerical Method

RAY Q. LIN AND NORDEN E. HUANG

Laboratory for Hydrospheric Processes, NASA/Goddard Space Flight Center, Greenbelt, Maryland

(Manuscript received 12 January 1994, in final form 9 May 1995)

ABSTRACT

To select a wind wave model as the basis for developing a coupled wind wave–current model for coastal dynamics, the numerical schemes used in state-of-the-art wind wave models are examined analytically. The schemes used in the existing models contain serious numerical aliases leading to dissipation and dispersion. These numerical aliases could mistakenly be interpreted as part of the physical phenomena. To alleviate these shortcomings, a fourth-order semi-implicit scheme for transport-type models and a second-order semi-implicit scheme with a gradient-dependent directional filter for the conservation-type models are proposed. The traditional difficulty of a hyperbolic conservation law is surmounted by this directional filter. These new schemes and the new filter are insensitive to the sizes of the time step and spatial grid and the magnitude of the group velocity; therefore, aliasing of the physical phenomena will not occur. Furthermore, the numerical dissipation and the dispersion of the new method are practically zero. Even though each computation step of these new schemes requires greater computing time, the total computing time is still considerably shorter than that in previous models because the time steps of the new schemes can be an order of magnitude greater than those used previously.

1. Introduction

Ever since Gelci et al. (1957) first tried to model wind-generated surface waves, many improved models have been developed (e.g., SWAMP Group 1985; SWIM Group 1985; WAMDI Group 1988). The state-of-the-art model is WAM (Günther et al. 1993). Almost all of the models have been designed for open oceans; the coastal region has been treated only cursorily. Surface gravity waves, whether generated locally by coastal weather or propagating onto the shelf as swell from distance storms, can greatly influence the wind stress distribution (Reider et al. 1994), which, in turn, can affect the nearshore flows and fundamentally modify the coastal dynamics. Furthermore, the wind is also very efficient in driving strong coastal currents near topographic features. These wind-driven currents can exert a strong influence on the surface gravity wave field, and they are very efficient in adjusting the mass field and surface temperature patterns. Due to the presence of the coast, the waves (as the drag causing roughness elements) are never homogeneous. Therefore, both the waves and the wind-driven currents can influence the atmospheric forcing. The coupling between atmospheric forcing, surface gravity waves, and wind-driven currents is a unique feature complicating study of the coastal region. To address the problems inherent to this coupled system, we have to develop a wind wave–current coupled coastal dynamics model.

As the first step, we need a workable coastal wind wave model, for the wind waves serve as the intermediary for the transfer of energy and momentum across the air–sea interface (e.g., see Phillips 1977). Since none of the existing models can fulfill this role, we decided to develop a new Goddard Coastal Wave Model (GCWM) for our purpose. As part of our effort, we have examined the state-of-the-art wind wave models critically by separating each component of the system and made the necessary changes for these models to work in the coastal region. In this paper we report our results concerning the design of new numerical schemes. To emphasize the effects of the numerics, we will discuss wave propagation only, and set the source function identically zero for the present.

The importance of the numerics in modeling is obvious. It can introduce computational dispersion and dissipation, which, if not properly accounted for, could be misinterpreted as part of the physical processes. Currently, there are two different approaches used in third-generation wave modeling: The first approach (e.g., WAM) uses the transport equation and employs the classic first-order Euler upstream scheme for swell propagation; the second approach (e.g., Tolman 1992a) uses the conservation equation and employs the ICN (iterative approximation of the Crank–Nicholson scheme)-center-space scheme. Neither of these two computing schemes is entirely satisfactory. Tolman (1992b) recently pointed out the problems with the nu-

Corresponding author address: Dr. Ray-Qing Lin, Code 5030, David Taylor Model Basin, Carderock Division, NSWC, Bethesda, MD 20084-5000.

merics of the WAM but offered no remedy. He ran the WAM model with different time steps and found differing results. These symptoms are precisely what should be expected: Since the waves are dispersive, the group velocity is a function of the frequency, the bottom topography, the current velocity, and even the local wave energy density N. Furthermore, since a wave model must deal with wideband spectra, it follows that the numerical dissipation and dispersion rates for different frequencies differ and their variation should be carefully monitored. The errors of wave propagation depend on the time step, grid size, and group velocity. These numerical errors can mix with the true physical phenomena and lead to false interpretations of the wave generation or evolution processes.

In this paper, we first examine analytically the problems associated with the presently used numerical schemes. Our results show that the first-order Euler upstream scheme for the transport equation, in the worst case, can transport only 20% of the initial energy density after one time step depending on the wavenumber, time step size, grid size, and location. As a result, when one changes the time step from 5 to 2 minutes maintaining the same grid size (Δx), the numerical solutions for some wave components can decrease 50%. We will also show analytically that the numerical solution of the ICN scheme is unconditionally computationally unstable for the conservation equation. Therefore, it not only grows exponentially with time but also generates a sizable numerical tail, which can reach about 40% of the original solution. Additionally, the oscillating computational mode can mix with the physical mode, thus rendering the purely physical mode difficult to interpret. The most serious problem with these numerical errors is that they differ for different wave components. With the extensive tuning used in the present models, these nonuniform variations of numerical dissipation and dispersion with respect to wavenumbers are impossible to separate from the consequences of real physical processes.

To alleviate all these difficulties, we propose a fourth-order semi-implicit scheme for the transport-type wind wave model and a second-order semi-implicit scheme with a gradient-dependent directional filter for the conservation-type wind wave model. This special directional filter guarantees the conservation of the propagating quantities. The new schemes provide several advantages: First, the inevitable numerical errors of whatever size are independent of the time step, grid size, and the group velocities. In other words, the numerical errors are uniform for all wave components; therefore, the differences between the numerical processes and the true physical processes can be easily separated. Second, the numerical dissipation and dispersion are practically nonexistent, and the propagating quantity is truly conserved. Finally, the time step in these new methods can be at least four times greater than in the previous schemes; therefore, the new method is about three times faster than the older methods. We will present all of these results analytically. Without loss of generality, however, we will present the analyses only for the one-dimensional case in this paper.

2. The numerical methods

In order to discuss the computational error quantitatively and analytically, we introduce two standard measuring parameters: the normalized solution, also known as the computational stability parameter $|\Lambda|$, and the normalized propagational velocity, also known as the computational dispersion parameter, $(c_g + u)^*/(c_g + u)$, in which c_g is the group velocity and u is the current. The computational stability parameter is defined as

$$|\Lambda| = |N^{n+1}/N^n|, \tag{1}$$

where N is the quantity to be computed and the superscript n or $n + 1$ is the number of the time step. When $|\Lambda| < 1$, the numerical scheme is computationally stable but damped (dissipative); when $|\Lambda| = 1$, the numerical scheme is computationally neutrally stable (nondissipative); when $|\Lambda| > 1$, the numerical scheme is computationally unstable. We will further use Λ_{true} as the stability parameter of the true solutions with $|\Lambda_{\text{true}}|$ always equal to 1.

The computational dispersion parameter is defined as

$$(c_g + u)^*/(c_g + u), \tag{2}$$

where $(c_g + u)^*$ is the computational velocity and $(c_g + u)$ is the true velocity. To obtain $(c_g + u)^*$, we must introduce a computational phase error θ^* as

$$-\theta^* = \tan^{-1}(-\Lambda_i/\Lambda_r), \tag{3}$$

where Λ_i is the imaginary part and Λ_r is the real part of Λ.

Another important computational parameter, the CFL condition μ, is defined as

$$\mu = (c_g + u)\Delta t/\Delta x, \tag{4}$$

in which Δt is the time step and Δx is the grid size. This parameter will appear in many of the analytic expressions of the computational analysis.

a. Transport equation

Since WAM uses the transport equation, we will examine that scheme first. Let N be the energy density spectrum; t the time; x, y the horizontal coordinates; θ the propagation angle; f the frequency; and S the sum of all the source functions. Furthermore, let $c_{gx} + u$, $c_{gy} + v$, $c_{g\theta}$, and c_{gf} be the propagation velocities of the energy density spectrum component in x, y, θ, and f space, respectively, in which u and v are the ambient current velocities and c_{gx} and c_{gy} are the group velocities

in the x and y directions, respectively. Thus, we have the basic transport equation for the energy spectrum of the wave field as

$$\frac{\partial N}{\partial t} + (c_{gx} + u)\frac{\partial N}{\partial x} + (c_{gy} + v)\frac{\partial N}{\partial y} + c_{g\theta}\frac{\partial N}{\partial \theta} + c_{gf}\frac{\partial N}{\partial f} = S. \quad (5)$$

We will set $S = 0$ identically in this paper. Furthermore, we also assume that $N = N(x, t)$; therefore, Eq. (5) will be simplified to a one-dimensional transport equation. However, the numerical results apply to the full multidimensional cases.

1) The classic Euler upstream scheme (first order)

The classic Euler upstream scheme is the straightforward conversion of a differential equation to the difference format, in which the temporal and spatial differences are related as follows:

$$\frac{N_j^{n+1} - N_j^n}{\Delta t} = (c_g + u)_j \frac{N_{j-1}^n - N_j^n}{\Delta x}, \quad (6)$$

where n is the number of the time step and j is the number of the grid point. To facilitate quantitative analysis of the numerical scheme, we assume $N_j = N_0 \exp[ik(j\Delta x - v_j t)]$, where N_0 is the value of the arbitrary gauging function at the boundary ($x = 0$), k is the wavenumber in space, and $v_j = (c_g + u)_j$. There is no loss of generality in adopting this form for N, for an arbitrary function can be expressed as its Fourier expansion. The important quantities here are the propagation speed and direction. With these substitutions, Eq. (6) becomes

$$N_j^{n+1} - N_j^n = [\mu_j(\cos k\Delta x - 1) - i\mu_j \sin k\Delta x]N_j^n. \quad (7)$$

In terms of the measuring parameters introduced above, Eq. (7) yields

$$\Lambda_j = \frac{N_j^{n+1}}{N_j^n} = \exp(-ikv_j\Delta t) = 1 + \mu_j(\cos k\Delta x - 1) - i\mu_j \sin k\Delta x; \quad (8)$$

therefore, the computational stability parameter is

$$|\Lambda|_j = [1 - 2\mu_j(1 - \mu_j)(1 - \cos k\Delta x)]^{1/2}, \quad (9)$$

the computational phase error is

$$-\theta_j^* = -\text{phase}(\Lambda) = kv_j\Delta t = \tan^{-1}\frac{\mu_j \sin k\Delta x}{1 + \mu_j(\cos k\Delta x - 1)} \overset{k\Delta x \to 0}{\to} \mu_j k\Delta x, \quad (10)$$

and the computational velocity is

$$(c_g + u)_j^* = \frac{-\theta_j^*}{k\Delta t} \overset{k\Delta x \to 0}{\to} (c_g + u)_j. \quad (11)$$

Thus, we obtain the analytic expression for the computational stability parameter in terms of $k\Delta x$ and μ_j.

Figure 1a shows how $|\Lambda|$ varies with $k\Delta x$ for different μ_j. Line A represents the true solution (Λ_{true}), lines B, C, D, E, F, G, H, I represent the numerical results for μ equal 0.2, 0.4, 0.707, 0.87, 1., 1.1, 1.2, 1.5 respectively. When $\mu_j = 0$ or 1, $|\Lambda| = \Lambda_{\text{true}} = 1$. Other than these two trivial values, whenever $\mu_j > 1$, $|\Lambda| > 1$, computational instability will occur. These situations should be avoided, for the solution will grow with time to infinity. Whenever $\mu_j < 1$, $|\Lambda| < 1$, computational dissipation will occur. For a fixed μ, when $\mu_j < 1$, the relative minima of $|\Lambda|$ occur at $k\Delta x = (2l + 1)\pi$, while the relative maxima of $|\Lambda|$ occur at $k\Delta x = 2l\pi$, with $l = 0, 1, 2, 3, \cdots$.

If $k\Delta x$ equals $(2l + 1)\pi$, the absolute minimum of $|\Lambda| = 0.2$ occurs when μ_j equals $\sqrt{2}/3$. This is the worst case, where the numerical solution of the classic Euler upstream scheme will be only 20% of the true solution after one time step. To avoid these pitfalls, one may be able to control Δt and Δx in the computation; however, for a finite bandwidth spectrum, one cannot control the wavenumber k, which, in turn, determines the group velocity through the dispersion relationship. Therefore, the classic Euler upstream scheme used in the WAM model may encounter serious nonuniform dissipative problems. With this interpretation, it becomes obvious why Tolman (1992b) found that the WAM gives different results for different Δt.

We can illustrate the above discussion with a simple example involving the propagation of a positive definite spectrum function given by a Gaussian pulse, $N^{(0)} = \exp\{-k[x - (c_g + u)t_0]^2\}$, where $k = 0.2$ and $t_0 = 10$. The results are computed based on the following values: $(c_g + u) = c_1 + c_2[1 + \cos(j\Delta x)]$, where c_1 and c_2 equal 0.6 and 0.2 respectively; $\Delta t_1 = 0.25$, $\Delta t_2 = 0.5$; $n_1 = 400$, $n_2 = 200$; $\Delta x = 0.5$. The maxima of $\mu_{(x)}^1$ and $\mu_{(x)}^2$ are 0.5 and 1.0 respectively; and the minima of $\mu_{(x)}^1$ and $\mu_{(x)}^2$ are 0.3 and 0.6 respectively.

Figure 1b shows the distribution of N when $t = 100$. Line A represents the true solution, while lines B and C represent the numerical solutions of the classic Euler upstream scheme for μ^1 and μ^2, respectively. The amplitudes of the numerical solutions are only 33% of the true solution for μ^1 and 28% of the true solution for μ^2. These results, though poor, are far from the worst case. Examples that are computationally unstable are not shown, for the solutions simply blow up. One may consider increasing the order of the Euler scheme to control the numerical errors. This approach is not viable, as will be shown presently.

2) Higher-order schemes

The properties of any higher, mth, order Euler upstream scheme can be derived as follows. First we have

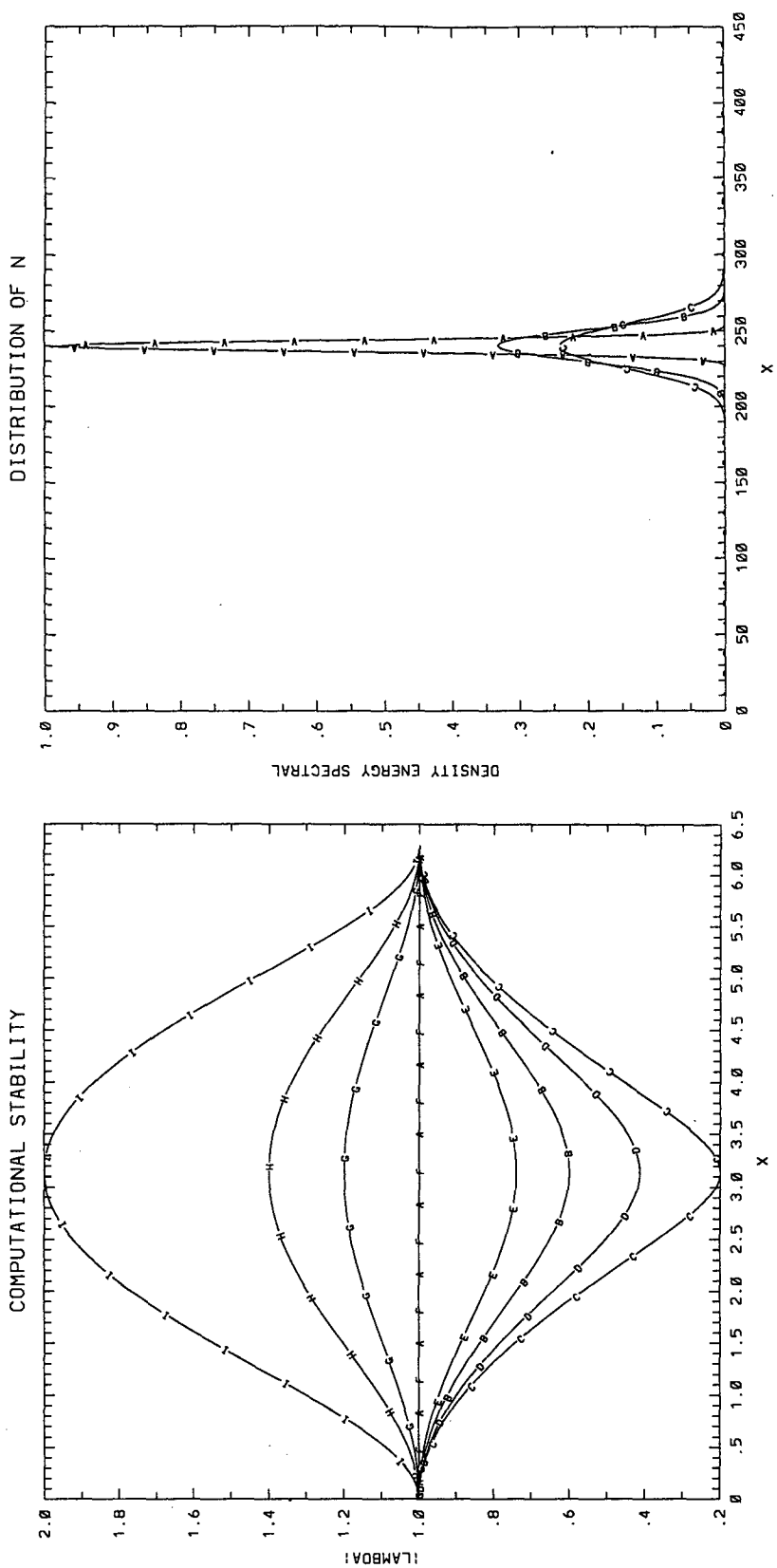

FIG. 1. (a: left) The computational instability parameters of the classic Euler upstream scheme for the transport equation, employed in the current WAM mode; $|\Lambda|$ varies with $k\Delta x$ for different μ: $\mu^B = 0.2$, $\mu^C = 0.4$, $\mu^D = 0.707$, $\mu^E = 0.87$, $\mu^F = 1.$, $\mu^G = 1.1$, $\mu^H = 1.2$, $\mu' = 1.5$. (b: right) Numerical dispersion and dissipation of the energy density spectrum N based on the classic Euler upstream scheme for the transport equation used in the current WAM model, when $t = 100$. The initial energy density spectral function is given by $N^{(0)} = \exp\{-k[x - (c_g + u)t_0]^2\}$, where $k = 0.2$, $t_0 = 10$, $(c_g + u) = c_1 + c_2[1 + \cos(j\Delta x)]$ ($c_1 = 0.6$, and $c_2 = 0.2$), and $\Delta x = 0.5$. Line A represents the true solution; line B represents the numerical solution, for $\Delta t = 0.25$, $n = 400$, the maximum μ is 0.5 and the minimum μ is 0.3; line C represents the computational solution, for $\Delta t = 0.5$, $n = 200$, the maximum μ is 1.0 and the minimum μ is 0.6.

$$N_j^{n+1} = \sum_{j'}^{m} a_{j'} N_{j+j'}^n, \tag{12}$$

in which $a_{j'}$ are constant coefficients to be determined by the normalization condition given later.

Using the Taylor expansions for N_j^{n+1} and $a_{j'}N_{j+j'}^n$, we then obtain

$$N_j^{n+1} = N_j^n + \Delta t \frac{\partial N_j^n}{\partial t} + \frac{(\Delta t)^2}{2}\frac{\partial^2 N_j^n}{\partial t^2} + \cdots \tag{13}$$

and

$$a_{j'}N_{j+j'}^n = a_{j'}\left[N_j^n + (j'\Delta x)\frac{\partial N_j^n}{\partial x} + (j'\Delta x)^2 \frac{\partial^2 N_j^n}{\partial x^2} + \cdots \right]. \tag{14}$$

By substituting Eqs. (13) and (14) into (12) and using $\partial N^n/\partial t = -(c_g + u)(\partial N^n/\partial x)$, we have

$$(1 - \sum_{j'} a_{j'})N_j^n + (-\mu - \sum_{j'} a_{j'})\Delta x \frac{\partial N_j^n}{\partial x} + \cdots + [(-\mu)^m - \sum_{j'} a_{j'} j'^m]\frac{\Delta x^m}{m!}\frac{\partial^m N_j^n}{\partial x^m} + O(\Delta x)^{m+1} = 0. \tag{15}$$

The higher-order computational parameters ($a_{j'}$, $j' = 1, 2, 3, \cdots, m$) can be derived for any order m provided that they satisfy the following necessary conditions:

$$\sum_{j'} a_{j'} = 1 \quad \text{and} \quad (-\mu)^m = \sum_{j'} a_{j'} j'^m, \qquad m = 1, 2, \cdots, m. \tag{16}$$

We will not show the details of the higher-order numerical solutions here. Our analysis, however, leads us to the following general conclusions. Simply increasing the order of a numerical scheme will not yield a better solution. Although higher-order schemes decrease numerical errors, numerical dissipation and dispersion continue to exist for any finite order. The rule is that dissipation dominates when m is odd and dispersion dominates when m is even. When m is greater than 2, the boundary condition becomes increasingly more complicated. The key to limiting numerical errors in any order of the Euler-upstream scheme is to use very small Δt, which unfortunately requires enormous amounts of computer time.

For wave research, there is another more serious shortcoming of the classic Euler upstream scheme, for we have to deal with problems with finite spectral bandwidth. In the finite bandwidth problem, the dissipation and dispersion will be nonuniform for different wave components. Such effects are impossible to separate from other real physical processes expressed in the various source functions, which are all wavenumber and frequency dependent. Based on these considerations, it becomes obvious that although the classic Euler upstream scheme was popular in earlier numerical studies of fluid mechanics problems, it no longer offers a viable choice, as shown by Press et al. (1989).

3) A NEW FOURTH-ORDER SEMI-IMPLICIT SCHEME

The idea of this new scheme is to use it implicitly to increase the accuracy of the computation instead of reducing the size of the gridpoint interval in space or time. To obtain an implicit scheme, we begin with the expression

$$\frac{N_j^{n+1} - N_j^n}{\Delta t} = -\frac{1}{2}\overline{(c_g + u)}_j^{xn}\left(\frac{\partial N_j^n}{\partial x} + \frac{\partial N_j^{n+1}}{\partial x}\right), \tag{17}$$

where $\overline{(\ )}^{xn}$ means averaging in Δx_j and Δt at $t = n\Delta t$. Therefore, $\partial\overline{(c_g + u)}^{xn}/\partial x = 0$. We are able to do so because Eq. (17) is the transport equation that does not include $\partial(c_g + u)/\partial x$. Using the Taylor expansion, we have

$$N^{n+1} = N^n + \Delta t\frac{\partial N^n}{\partial t} + \frac{\Delta t^2}{2}\frac{\partial^2 N^n}{\partial t^2} + \frac{\Delta t^3}{3!}\frac{\partial^3 N^n}{\partial t^3} + \cdots, \tag{18}$$

and

$$N^n = N^{n+1} - \Delta t\frac{\partial N^{n+1}}{\partial t} + \frac{\Delta t^2}{2}\frac{\partial^2 N^{n+1}}{\partial t^2} - \frac{\Delta t^3}{3!}\frac{\partial^3 N^{n+1}}{\partial t^3} + \cdots. \tag{19}$$

Subtracting Eq. (19) from Eq. (18), we obtain

$$N^{n+1} - N^n = \frac{\Delta t}{2}\left(\frac{\partial N^n}{\partial t} + \frac{\partial N^{n+1}}{\partial t}\right) + \frac{\Delta t^2}{4}\left(\frac{\partial^2 N^n}{\partial t^2} - \frac{\partial^2 N^{n+1}}{\partial t^2}\right) + \frac{\Delta t^3}{12}\left(\frac{\partial^3 N^n}{\partial t^3} + \frac{\partial^3 N^{n+1}}{\partial t^3}\right). \tag{20}$$

From Eq. (5), we may write

$$\frac{\partial N^n}{\partial t} = -\overline{(c_g + u)}^{xn}\frac{\partial N^n}{\partial x} = -\frac{\partial F^n}{\partial x}, \tag{21a}$$

$$\frac{\partial^2 N^n}{\partial t^2} = \frac{\partial}{\partial t}\left(-\frac{\partial F^n}{\partial x}\right) = -\frac{\partial}{\partial x}\left(\frac{\partial F^n}{\partial t}\right) = \frac{\partial}{\partial x}\left\{[\overline{(c_g + u)}^{xn}]^2\frac{\partial N^n}{\partial x}\right\}, \tag{21b}$$

where $F^n = \overline{(c_g + u)}^{xn} N^n$. Similarly,

$$\frac{\partial N^{n+1}}{\partial t} = -\overline{(c_g + u)}^{xn} \frac{\partial N^{n+1}}{\partial x} = -\frac{\partial F^{n+1}}{\partial x}, \quad (22a)$$

$$\frac{\partial^2 N^{n+1}}{\partial t^2} = \frac{\partial}{\partial x}\left\{[\overline{(c_g + u)}^{xn}]^2 \frac{\partial N^{n+1}}{\partial x}\right\}, \quad (22b)$$

where $F^{n+1} = \overline{(c_g + u)}^{x} N^{n+1}$. Substituting Eqs. (21b) and (22b) into the third-order term of Eq. (20), we obtain

$$\frac{\partial^3 N^n}{\partial t^3} + \frac{\partial^3 N^{n+1}}{\partial t^3} = \frac{\partial}{\partial x}\left\{[\overline{(c_g + u)}^{xn}]^2 \frac{\partial}{\partial x} \times \left[\frac{\partial N^n}{\partial t} + \frac{\partial N^{n+1}}{\partial t}\right]\right\}. \quad (23a)$$

Recalling the first-order term of Eq. (20),

$$N^{n+1} - N^n = \frac{\Delta t}{2}\left(\frac{\partial N^n}{\partial t} + \frac{\partial N^{n+1}}{\partial t}\right),$$

and substituting it into Eq. (23a), we arrive at the following equation:

$$\frac{\partial^3 N^n}{\partial t^3} + \frac{\partial^3 N^{n+1}}{\partial t^3} = \frac{\partial}{\partial x}\left\{[\overline{(c_g + u)}^{xn}]^2 \frac{\partial}{\partial x} \times \left[\frac{2}{\Delta t}(N^{n+1} - N^n)\right]\right\}. \quad (23b)$$

Now, substituting Eqs. (21), (22), and (23) into (20), we obtain the new semi-implicit scheme as

$$\left\{1 + \frac{\Delta t}{2}\overline{(c_g + u)}^{xn}\frac{\partial}{\partial x} + \frac{\Delta t^2}{12}\frac{\partial}{\partial x}[\overline{(c_g + u)}^{xn}]^2 \frac{\partial}{\partial x}\right\} N^{n+1} = \left\{1 - \frac{\Delta t}{2}\overline{(c_g + u)}^{xn}\frac{\partial}{\partial x} + \frac{\Delta t^2}{12}\frac{\partial}{\partial x}[\overline{(c_g + u)}^{xn}]^2 \frac{\partial}{\partial x}\right\} N^n. \quad (24)$$

Because the transport equation does not include $\partial(c_g + u)/\partial x$, we can assume that

$$\overline{(c_g + u)}^{jn} = \overline{(c_g + u)}^{(j+1/2)n} = \overline{(c_g + u)}^{(j-1/2)n} = \frac{1}{4}\overline{(c_g + u)}^{(j+1)n} + \frac{1}{2}\overline{(c_g + u)}^{jn} + \frac{1}{4}\overline{(c_g + u)}^{(j-1)n},$$

$$\frac{\partial}{\partial x}\left\{[\overline{(c_g + u)}^{xn}]^2 \frac{\partial N}{\partial x}\right\} = [\overline{(c_g + u)}^{xn}]^2[N_{j+1} + N_{j-1} - 2N_j]/(\Delta x)^2, \quad (25)$$

and

$$\overline{(c_g + u)}^{xn}\frac{\partial N}{\partial x} = \overline{(c_g + u)}^{jn}[N_{j+1} - N_{j-1}]/(2\Delta x). \quad (26)$$

Therefore, Eq. (24) can be rewritten as

$$\left\{\frac{\mu^{(n)}}{4}\left(\frac{\mu^{(n)}}{3} + 1\right)\right\}N_{j+1}^{(n+1)} + \frac{\mu^{(n)}}{4}\left(\frac{\mu^{(n)}}{3} - 1\right)N_{j-1}^{(n+1)} + \left(1 - \frac{\mu^{(n)2}}{6}\right)N_j^{(n+1)} = \left\{\frac{\mu^{(n)}}{4}\left(\frac{\mu^{(n)}}{3} - 1\right)\right\}N_{j+1}^{(n)} + \frac{\mu^{(n)}}{4}\left(\frac{\mu^{(n)}}{3} + 1\right)N_{j-1}^{(n)} + \left(1 - \frac{\mu^{(n)2}}{6}\right)N_j^{(n)}. \quad (27)$$

To analyze the computational errors, we substitute the same Fourier mode $\exp(ikj\Delta x)$ into Eq. (27) and obtain

$$\left\{1 + \frac{1}{12}(\mu^{(n)})^2[e^{ik\Delta x} + e^{-ik\Delta x} - 2] + \frac{1}{4}\mu(n)_j[e^{ik\Delta x} - e^{-ik\Delta x}]\right\}N_j^{n+1} = \left\{1 + \frac{1}{12}(\mu^{(n)})^2[e^{ik\Delta x} + e^{-ik\Delta x} - 2] - \frac{1}{4}\mu_j^{(n)}[e^{ik\Delta x} - e^{-ik\Delta x}]\right\}N_j^n, \quad (28)$$

where $\mu_j^n = \overline{(c_g + u)}^{j(n)}\Delta t/\Delta x$. Let us define

$$a = 1 - \frac{1}{3}(\mu^{(n)})^2 \sin^2\frac{k\Delta x}{2},$$

$$b = \frac{1}{2}\mu_j^{(n)} \sin k\Delta x.$$

Then, the computational stability parameter Λ can be shown to be

$$\Lambda = \frac{a - ib}{a + ib} = \frac{a^2 - b^2 - i2ab}{a^2 + b^2}. \quad (29)$$

Therefore, we always have

$$|\Lambda| = |\Lambda_{\text{true}}| = 1. \quad (30)$$

Equation (30) means that the new scheme is unconditionally and computationally neutrally stable (nondissipative) for all μ. If we wanted to plot a computational stability graph as in Fig. 1a for the new scheme, the result would be a single line at $|\Lambda| = 1$.

For the asymptotic limit $k\Delta t \to 0$,

$$\Lambda = 1 + i\mu k\Delta x - \frac{1}{2}\mu^2(k\Delta x)^2 - i\frac{1}{6}\mu^3(k\Delta x)^3 + \frac{1}{24}\mu^4(k\Delta x)^4 + \cdots. \quad (31)$$

Unlike the explicit schemes, Eq. (31) shows that two levels of time and three grid points in space give us a fourth-order accuracy scheme instead of a second-order accuracy scheme.

For the numerical dispersion analysis, we obtain the computational phase error as

$$-\theta^* = \tan^{-1}\left(\frac{2ab}{a^2 - b^2}\right) \overset{k\Delta x \to 0}{\to} (c_g + u)k\Delta t \Rightarrow$$

$$(c_g + u)^* = -\theta^*/k\Delta t \overset{k\Delta x \to 0}{\to} (c_g + u). \quad (32)$$

When the grid size is small, the dispersion will be eliminated. Unlike the Euler upstream scheme, Δt can still be reasonably large for a small Δx. Therefore, we can also limit the dispersion by using this fourth-order semi-implicit scheme. Figure 2 is the same as Fig. 1b except that it presents results for the fourth-order semi-implicit scheme. The maxima of the numerical solutions from the fourth-order semi-implicit scheme are about 73% of the true solution for both μ^1 and μ^2 when $t = 100$. If we increase μ by a factor of 2, the computational amplitude is still about 73% of the true solution. It should be pointed out that the decrease in the maximum here is not due to dissipation, for this scheme is nondissipative; rather, it is due to dispersion, which causes the same amount of energy to spread out. The results of the large μ shown here cannot be obtained from any of the previous schemes because they suffer from computational stability problems.

Based on these comparisons, we conclude that the new scheme is superior to the classic Euler upstream scheme. The reasons can be reiterated as follows: First, the new scheme eliminates computational dissipation completely for all μ and limits the dispersion to an acceptable level for a reasonably large Δt and small Δx. The numerical errors of the implicit scheme are practically independent of μ. The dispersion effect does change the distribution of the solution slightly, but there are no significant negative values of N. Therefore, the new scheme presented here gives more reliable numerical solutions and also saves computing time. Second, the new scheme generates only a physical mode. Third, one has only to deal with a simple boundary condition in this implicit high-order scheme, which is different from the case with classic high-order schemes.

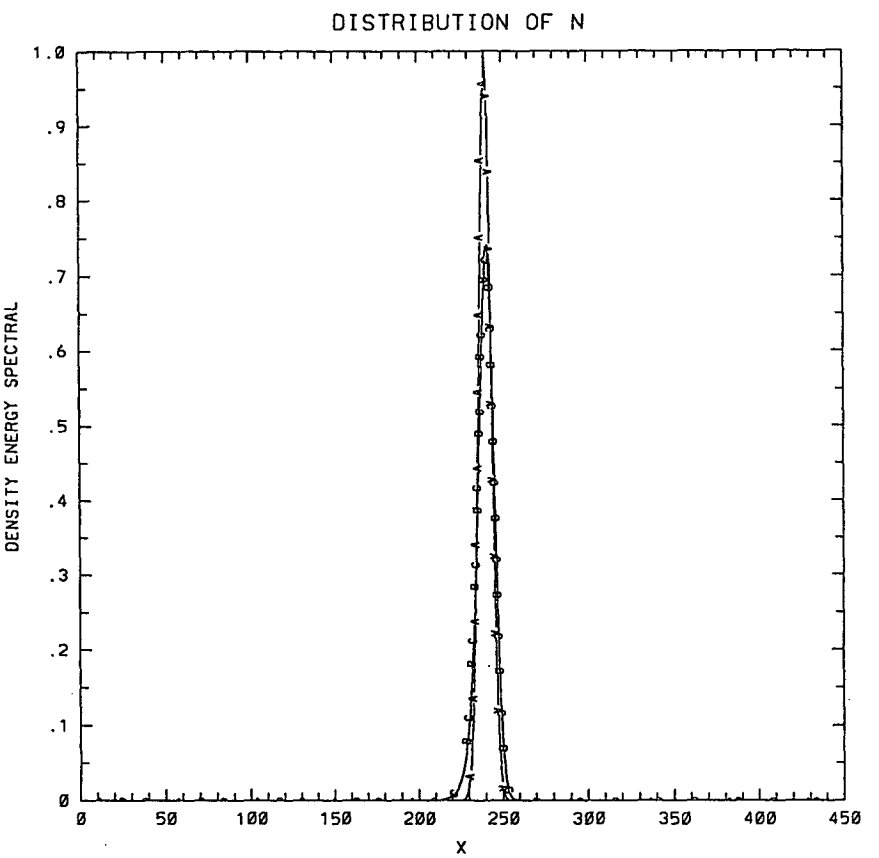

FIG. 2. Same as Fig. 1 except that the numerical computation here is based on the fourth-order semi-implicit scheme.

And finally, unlike the Taylor–Galerkin method (Chen 1992), one only has to solve a narrow-band matrix by using a preconditional conjugate residual method (Lin et al. 1992) instead of a full matrix, which again results in computational time savings. Based on dynamical considerations, the transport equation should not be used. If for some special reason the transport equation is preferred, the fourth-order semi-implicit scheme should be adopted.

b. Conservation equation

Having discussed the different schemes for the transport equation, we now consider the conservation type of equation

$$\frac{\partial A}{\partial t} + \frac{\partial[(c_{gx} + u)A]}{\partial x} + \frac{\partial[(c_{gy} + v)A]}{\partial y} + \frac{\partial[c_{g\theta}A]}{\partial \theta} + \frac{\partial[c_{gf}A]}{\partial f} = S, \quad (33)$$

in which A is the spectral action density, defined as the ratio of spectral energy density to the intrinsic frequency. Although all the computations are performed in terms of the action density, the final results are converted into spectral energy density because it is a directly observable quantity.

There are two major advantages of using the conservation law in wave modeling. First, action conservation is the most fundamental law governing the wave motion. The conservation of action can be shown to be equivalent to the conservation of energy only when the intrinsic frequency is an invariant following the waves. In coastal regions where the bottom topography changes from one location to another and unsteady tidal currents prevail, the intrinsic frequency is no longer an invariant and the wave energy density is no longer conserved. The conserved quantity is the action density that is equivalent to the energy flux. Under these conditions, the action conservation law is preferable. The second, more practical, reason is to accommodate the effects of currents. To account for the ubiquitous coastal tidal currents in the transport equation requires the inclusion of the radiation stress, which is rather cumbersome to compute. But in the action conservation equation, the current–wave interaction is included easily. The action conservation equation used here is the same as that in Tolman (1992a). The difference is that we do not invoke the conservation of wave crests as did Tolman (1992a). The advantage of the conservation-type equation, however, can be easily offset by a well-known difficulty: the difficulty in finding a usable numerical scheme that will conserve the total action in a hyperbolic conservation law. This difficulty was partially resolved by sophisticated methods in a one-dimensional case (Shu and Osher 1989). For more general multidimensional cases, the solutions are still elusive. We will introduce a new method that will be applicable to the specific conservation equation in a multidimensional domain as required by Eq. (33).

For the conservation equation [Eq. (33)], the Euler upstream scheme becomes unconditionally computationally unstable because $\partial_x(c_{gx} + u) \neq 0$ (Book et al. 1975). For the same reason, the special fourth-order implicit scheme discussed above and the ICN scheme used by Tolman (1992b) suffer the same defect as the Euler upstream scheme.

To overcome this difficulty, we propose a second-order semi-implicit scheme with a directional filter. This scheme will be discussed and compared with the ICN scheme used by Tolman (1992b). For simplicity, we will treat the one-dimensional case analytically as before. The numerical results, however, are for the full multidimensional cases.

1) THE ICN SCHEME

The finite-difference expression for the ICN scheme is

$$A_j^{n+1} - A_j^n = \frac{\Delta t}{2\Delta x}\{(1 + \alpha)[(c_g + u)A]_{j-1} - 2\alpha[(c_g + u)A]_j - (1 - \alpha)[(c_g + u)A]_{j+1}\}^n, \quad (34)$$

where α is a parameter within the range $0 \leq |\alpha| \leq 1$, which is used to determine the relative importance of the propagation and source terms. Note that the sign of α is chosen to be the same as of that $c_g + u$. Phillips (1959) has demonstrated that this type of scheme is unconditionally computationally unstable, a fact fully acknowledged but also ignored by Tolman (1992a). In an effort to alleviate this problem, Tolman (1992a) used parameter α. When α is small, the propagation term dominates. When α is large, the source term dominates. Therefore, the ICN scheme remains unconditionally computationally unstable unless α is large enough to stabilize the propagation terms by allowing the source terms to become dominant (Tolman 1992a). Tolman (1992b) also applied flux corrected transport as proposed by Book et al. (1975, 1981) and Boris and Book (1973, 1975, and 1976) in order to overcome the above problem. However, the flux corrected transport method is nothing but a numerical diffusion; it is unable to completely eliminate the above problem. Furthermore, the flux-corrected transport introduces new errors. The errors can be eliminated or controlled only for particular problems where the character of the solution is essentially known in advance (Book et al. 1974). Figure 3 shows the numerical simulation for N when $t = 100$. The solution is the same as that in Fig. 1b except that it is for the ICN scheme with $\alpha = 0$; and a set of much smaller $\Delta t = 0.1$, 0.05, and 0.0125. As noted above, unlike the numerical solutions of the transport equation (1), the solutions are unstable,

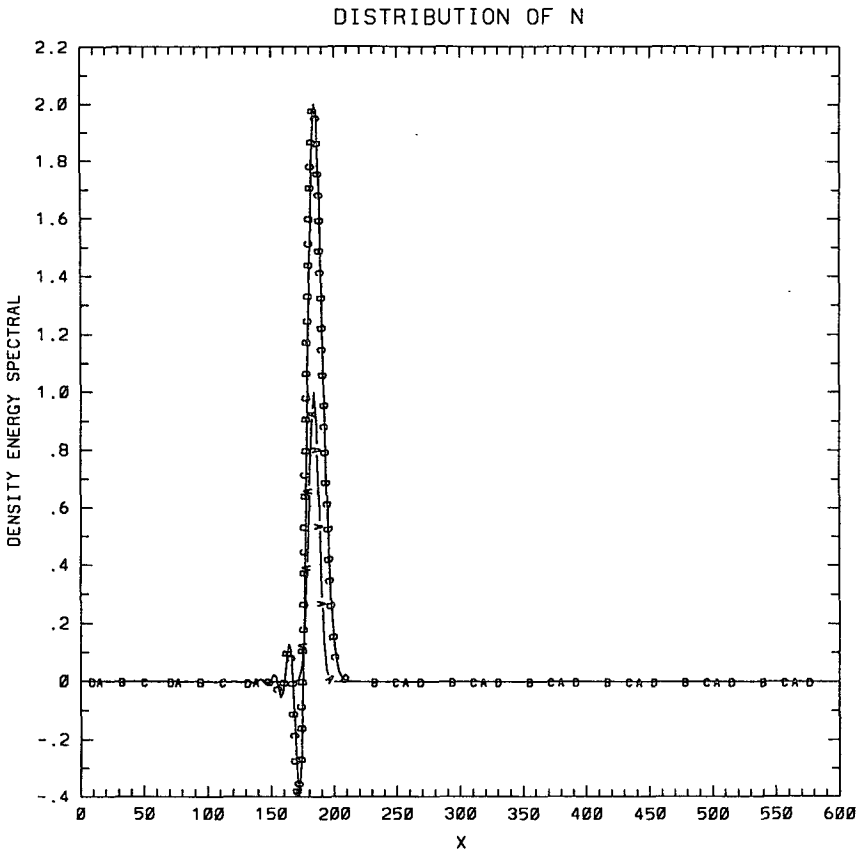

FIG. 3. Same as Fig. 1 except that the numerical computation here is based on the ICN scheme with ($\alpha = 0.0$) and conservation equation [Eq. (33)]. Line A represents the true solution; line B represents the numerical solution for $\Delta t = 0.1$ and $n = 1000$; line C represents the numerical solution for $\Delta t = 0.05$ and $n = 2000$; line D represents the numerical solution for $\Delta t = 0.0125$ and $n = 8000$.

and they grow to twice the magnitude of the real solution after $t = 100$. Additionally, there is a substantial amount of numerical dispersion. The tail of the noise dispersion can reach 40% of the true solution. Tolman applied the flux-corrected transport method to eliminate these noise tail problems by setting all the negative values to zero. Unfortunately, this simple solution did not eliminate the problem; there is a subtle difficulty here. Negative noise for a nonnegative function can, of cause, be eliminated easily, but there is no guarantee that some of the positive values are not spurious. These major drawbacks (high dispersion, unconditional computational instability, and the difficulty of separating the signal from the computational noises) have prompted Kriess and Lorenz (1990) to caution against the use of this scheme for hyperbolic-type equations.

2) SECOND-ORDER SEMI-IMPLICIT SCHEME

To solve the conservation equation, we propose two semi-implicit schemes designated as A and B. Type A is the formal semi-implicit scheme

$$A_j^{n+1/2} - A_j^n = (F_{j-1}^n - F_j^n)/2, \tag{35}$$

$$A_j^{n+1} - A_j^n = (F_{j-1}^{n+1/2} - F_j^{n+1/2}) * factor + (F_{j-1}^n - F_j^n) * (1 - factor), \tag{36}$$

where $F_j^n = (\Delta t/\Delta x)(c_g + u)_j A_j^n$ and $0 <$ factor < 1. Our study of the wave model indicates that the minimal numerical dissipation occurs when the *factor* is 0.7.

To conserve computation time, we also introduce a variety of the Type A scheme designated as Type B, in which

$$A_j^{n+1} - A_j^n = \frac{1}{2}[(F_{j-1}^{n+1} - F_j^{n+1}) + (F_{j-1}^n - F_j^n)]. \tag{37}$$

The stability parameter is

$$\Lambda = \frac{(1-a) - ib}{(1+a) + ib},$$

$$|\Lambda| = \frac{(1-a)^2 + b^2}{(1+a)^2 + b^2}, \tag{38}$$

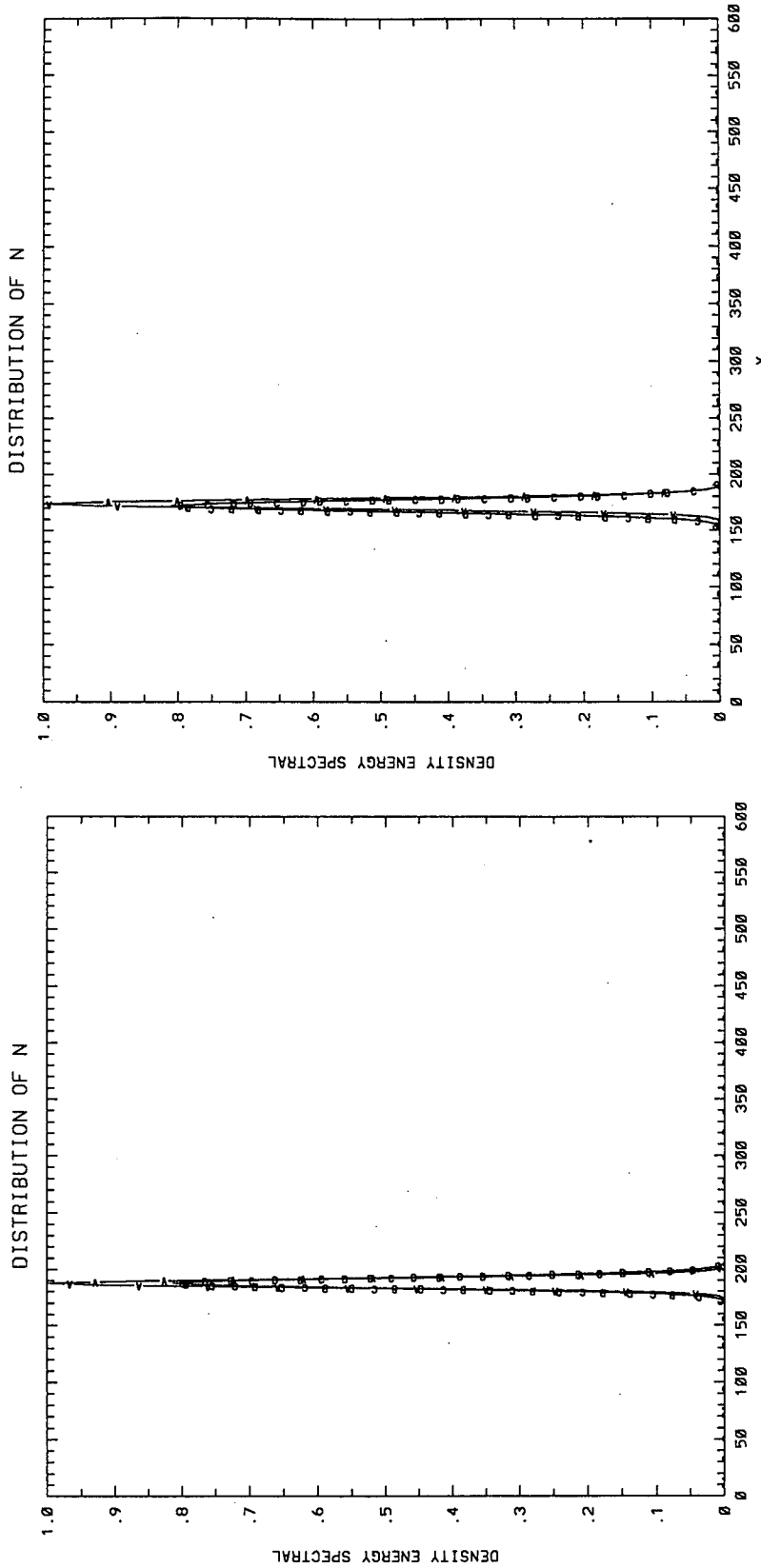

FIG. 4. Same as Fig. 3 except that it is for the second-order semi-implicit scheme and $\Delta t = 1.0$, 0.5, and 0.125, which are ten times greater than the ICN scheme (a: left) for Eqs. (35) and (36) with a directional filter and (b: right) for Eq. (37) with a directional filter.

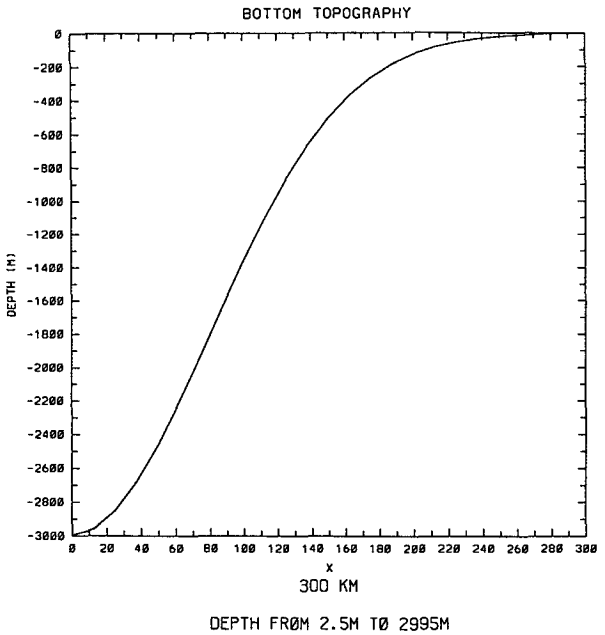

FIG. 5. The profile of bottom topography along the x direction for the test region.

where

$$a = \frac{\mu_j}{2} - \frac{\mu_{j-1}}{2} \cos k\Delta x$$

and

$$b = \frac{\mu_{j-1}}{2} \sin k\Delta x.$$

The dispersion parameter is

$$-\theta^* = \tan^{-1} \frac{b}{(1-a)} \overset{k\Delta x \to 0}{\to} \mu k\Delta x.$$

Therefore,

$$(c_g + u)^* = \frac{-\theta^*}{k\Delta t} \overset{k\Delta x \to 0}{\to} c_g + u. \qquad (39)$$

From Eq. (38), one can see that second-order semi-implicit schemes are stable when $a \geq 0$, and when $\mu \leq 0.5$, $100\% \geq |\Lambda| \geq 90\%$. Therefore, the computational dissipation is very small and does not vary significantly with μ when $\mu \leq 0.5$. Equation (39), however, indicates that this scheme is dispersive and nonconservative when $k\Delta x \neq 0$. Unlike the ICN scheme, the dispersion will not generate a sign changing tail, but it will spread action around the propagated direction and cause the total action to increase. Nonconservation of action is a classical difficulty encountered in numerical solutions of hyperbolic conservation equations. To compensate for the nonconservative property, we introduce a directional filter to maintain conservation of action. The filter forces total action to be conserved and suppresses numerical dispersion by a weighting function. This filter is not related to Δt, Δx, $(c_g + u)$, or μ. A more detailed description is given in the appendix.

The Type B scheme is twice as fast as for Type A. This gain in computational speed is paid for in accuracy. Our tests suggest that the accuracy of the Type B scheme is 5% less than that for Type A. Figure 4 shows that the distribution of N for the Type A and B schemes in the same format as Fig. 3 except that it is for the second-order semi-implicit scheme and $\Delta t = 1.0$, 0.5, and 0.125, which are ten times greater than the Δt in Fig. 3. Figure 4a is for Type A based on Eqs. (35) and (36), and Fig. 4b is for Type B based on Eq. (37) both with the directional filter. Figures 4a,b show that both numerical simulations are computationally stable; the maximum values equal about 83% of the true solutions when $t = 100$. The total energy remains the same and the results do not vary significantly with Δt, Δx, and $c_g + u$ when μ is less than unity.

3. Numerical results of wave propagation

In numerical computations, the equation types and kinematics influence the results. Therefore, a detailed comparison between WAM and Goddard Coastal Wave Models will be discussed separately in Part II. Here, we only compare the numerical simulations for the GCWM with and without a directional filter.

The numerical simulations were conducted in a rectangular box 300 km (in the x direction) $\times$ 900 km (in the y direction) with open boundaries. Along the x (west to east) direction, the depth of the ocean decreases from 3000 m to 2.5 m. The depth is uniform in the y (south to north) direction. Figure 5 shows this bottom topography. The spatial grid interval (Δx and Δy) is 12.5 km; the time step (Δt) is 10 min; the resolution for the propagation direction ($\Delta\theta$) is 30°; and the frequency resolution (Δf) is 0.1 f Hz. We assume a simple tidal current with a period of 24 h oscillating along the x direction. The magnitude of the tidal current is 0.2 m s^{-1} in the deep ocean and increases linearly to a maximum value of 1 m s^{-1} at the coastline. A continuous swell system enters only on the western boundary with the directional and frequency distribution illustrated in Fig. 6a. All other boundaries are open for the waves to propagate through without impedance. The numerical simulations are all applied to the pure propagation problem without source terms with the results in different directions presented according to the numbered system given in Fig. 6b.

The experiment was conducted numerically for 14 days. The test condition is so chosen to guarantee that the results represent the case of infinite long beaches with uniform open ocean boundary conditions. Figures 7a,b show the wave energy density spectra distribution over a whole tidal cycle along the direction number 4

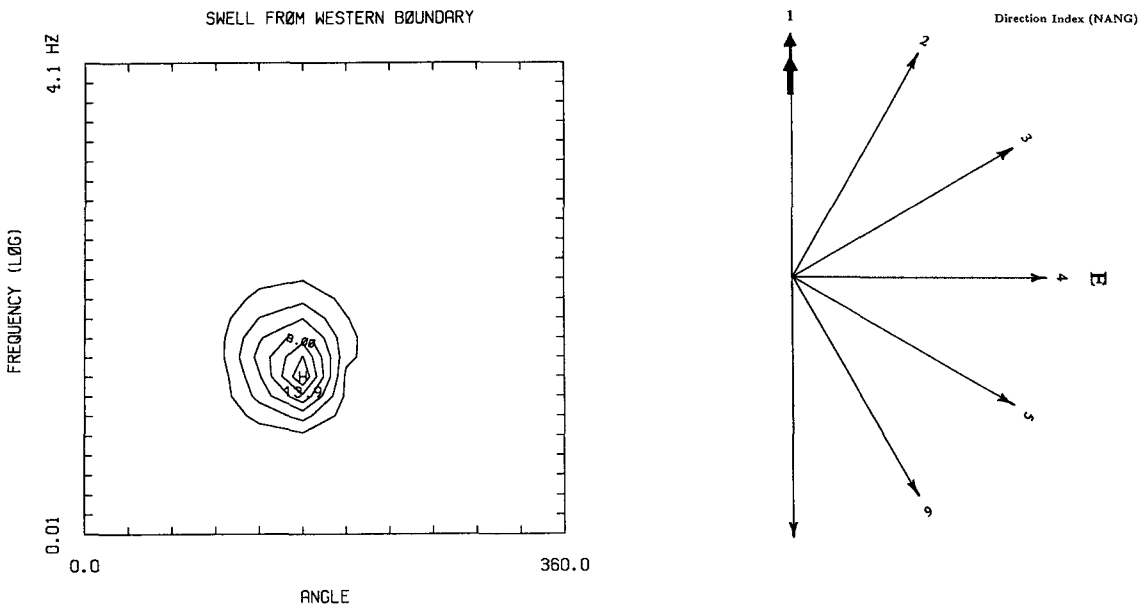

FIG. 6. (a) The direction energy spectrum of a swell system used in the propagation test. (b) The energy propagation direction labeled by a number system used in the computation.

and a line 100 km north of the southernmost boundary of the test region. In these figures, the horizontal axis indicates the distance from the coastline; the vertical axis indicates the wave frequency in Hz.

Figure 7a shows the results from the second-order implicit scheme without the directional filter. In this computation, action was first computed, and the results were then converted into energy density. The most conspicuous features are the drastic pileup of energy at the coastline, which agrees well with the analytical solution, as shown in Phillips (1977), and the widespread of energy over frequency space. Not all of the energy pileup is real, for this scheme does not conserve the total action. Therefore, the results could be exaggerated, yet there should be a drastic pileup as dictated by the analytical solution (Phillips 1977). The spreading of the energy density is no doubt due to computational dispersion in this scheme.

Figure 7b shows the results from the second-order implicit scheme with the special directional filter, which serves to eliminate the dispersion and to conserve the total action. The changes are quite drastic. The frequency spreading is much reduced, yet the energy pileup is retained. The lack of frequency spreading is to be expected, for with the linear dispersion relationship, the frequency should be nearly constant. As a result, the final width of the spectrum is almost equal to the original value. The amount of the energy pileup is slightly reduced as a consequence of the elimination of dispersion and the maintenance of the action conservation.

In reality though, the energy pileup could not have been as strong as depicted here, for some of the energy would inevitably be dissipated through bottom friction and wave breaking. But such physical effects are not included in any of the present computations; therefore, the pileup should be there as predicted by the analytical results in Phillips (1977). True physical processes will have to be invoked to dissipate some energy, but that is a separate issue from the computational dissipation addressed here. The simple comparisons presented here offer strong evidence for us to question the suitability of the propagation schemes used in previous models. Yet the numerical results from the implicit scheme with a directional filter confirm the analytic solutions. Thus, it is our view that the new numerical scheme should be adopted for a wave model either in terms of transport type or conservation type of equations.

4. Summary

To advance our understanding of wind wave field generation and evolution, a numerical model is a valuable tool; yet, in order for the tool be reliable, the underlying numerical scheme first has to be reliable. As our analyses show, numerical errors can cause not only quantitative but also qualitative errors. Such errors could cause computational effects to be misinterpreted as part of the true physical mechanisms. Clearly, without a reliable numerical scheme, the numerical errors will be intertwined with the true physical variations and adversely influence the form and substance of the kinematics and dynamic source functions.

Based on our analyses, we conclude that the first-order Euler upstream method contained in the WAM should not be used as a research tool, because it is strongly computationally dissipative and dispersive. But the WAM model is still better than the ICN scheme

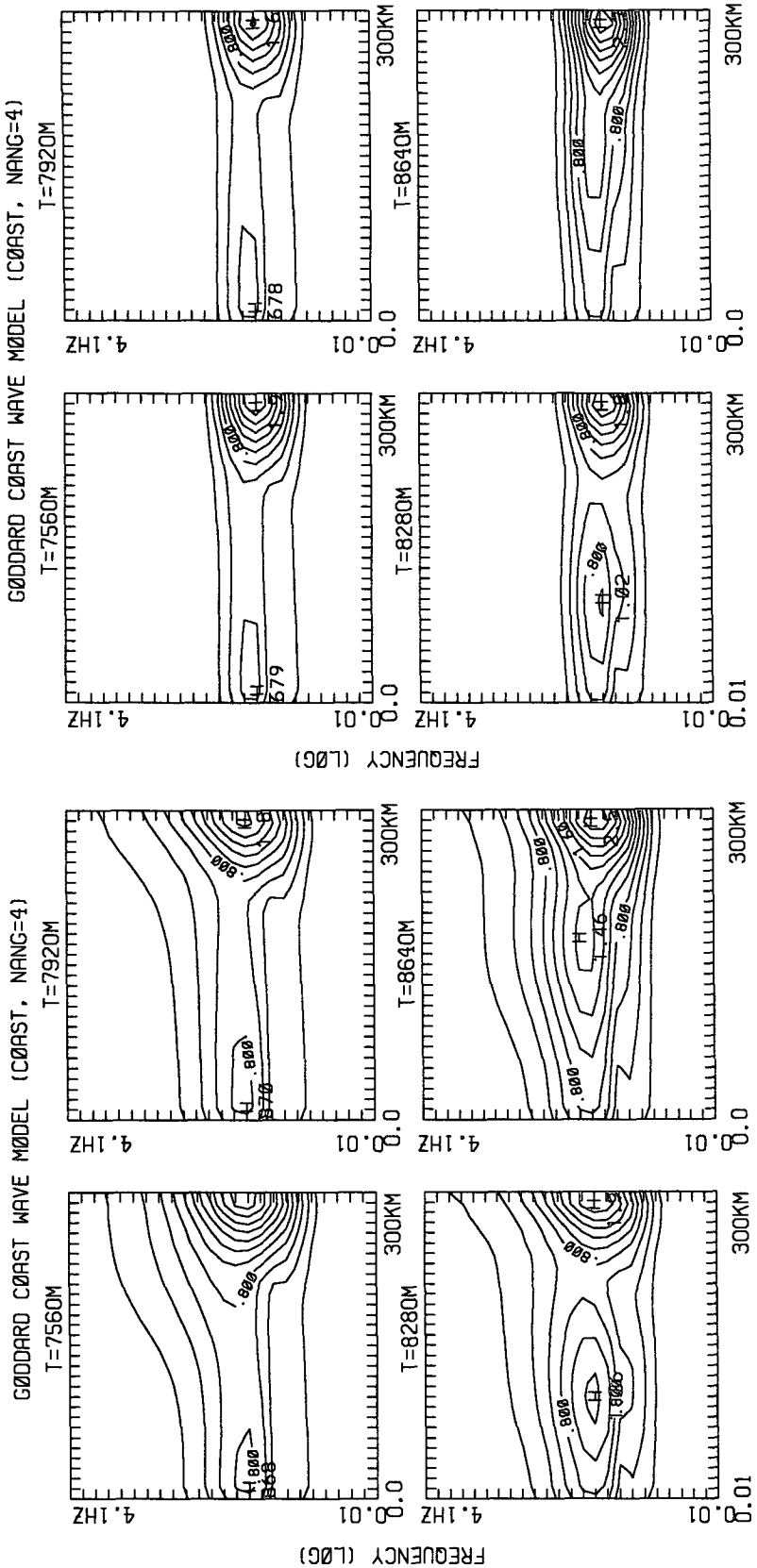

FIG. 7a. The numerical simulation of the energy density spectrum using the conservation equation and second-order semi-implicit scheme without the directional filter.

FIG. 7b. The numerical simulation of the energy density spectrum using the conservation equation and second-order semi-implicit scheme with the directional filter.

proposed by Tolman (1992a), for the ICN scheme in the conservation equation is unconditionally computationally unstable and strongly dispersive (see, e.g., Kriess and Lorenz 1990). Furthermore, an inseparable computational mode always occurs with the physical mode.

Wave modeling has advanced steadily through the years to the present state of sophistication. To proceed further, the need for a new scheme is absolutely essential and imperative. To this end, we proposed two alternatives: a fourth-order semi-implicit scheme for the transport-type equation, and the second-order semi-implicit scheme plus a directional filter for the conservation-type equation. Based on physical considerations, the second-order semi-implicit scheme for the action conservation equation should be used. On the practical side, the new schemes use much larger computational steps than the previous models. Therefore, the new methods use much less computational time than the previous models for the same conditions. The new schemes also overcome most of the previous numerical problems by limiting computational dissipation and dispersion. Most importantly, the new schemes are not significantly dependent on the group velocity, temporal step, or spatial grid size. Only by eliminating the computational dissipation and dispersion can one truly determine the effects of the physical processes.

Acknowledgments. We would like to express our deep appreciation for the kind help and discussions with Dr. H. S. Chen of NWC/NOAA and Dr. Steven Long of WFF/GSFC/NASA. This research has been supported by NASA Physical Ocean Program and the Coastal and Physical Oceanography Programs of the Office of Naval Research.

APPENDIX

Directional Filter

The directional filter is adopted to maintain the total action conservation. In a numerical solution of a differential equation in a multidimensional domain, it is necessary to take turns simulating each dimension while keeping the other dimensions frozen for the A-grid distribution, except in the ENO method (Shu and Osher 1989). The directional filter introduced here serves exactly this purpose as in the ENO method, but the directional filter is designed for multidimensional problems. The details of the directional filter will be discussed in a separate paper. We will offer the following outline to explain the essential features and the design principles of this filter. In a conservation equation of the type given by Eq. (33), we assume the original total action, $\mathrm{TA}^{(n)}$, to be

$$\mathrm{TA}^{(n)} = \sum_{j=1}^{L} A_j^{(n)},$$

in which n represents the time step, j represents the gridpoint number, and L is total number of grids. After m time steps, the total energy will be

$$\mathrm{TA}^{(n+m)} = \sum_{j=1}^{L} A_j^{(n+m)}.$$

If the action energy at each grid is conserved after m time integrations, then we will have the following equation:

$$\mathrm{filter}_j^{(n+m)}(A_j^{(n+m)} - FF_j^{(n+m/2)}\Delta t) = A_j^{(n)}, \quad \text{(A1)}$$

in which

$$FF_j^{(n+m/2)} = -\nabla\cdot(\mathbf{c}_g + \mathbf{u})_j^{(n+m/2)} A_j^{(n+m/2)} + \mathrm{forcing}_j^{(n+m/2)},$$

where forcing represents the source functions, which are assumed to be zero here. Equation (A1) can be rewritten for total action as

$$\sum_{j=1}^{L} \log_{10}\mathrm{filter}_j^{(n+m)} + \sum_{j=1}^{L} \log_{10}(A_j^{(n+m)} - FF_j^{(n+m/2)}\Delta t) = \sum_{j=1}^{L} \log_{10} A_j^{(n)}. \quad \text{(A2)}$$

We assume the $\mathrm{filter}_j^{(n+m)}$ to be a highly directional function in terms of $\cos^2\alpha_j$ and define the filter as

$$\mathrm{filter}_j^{(n+m)} = \begin{cases} [\cos^2\alpha_j]^{rr^{(n+m)}}, & \cos\alpha_j > 0 \\ 0, & \cos\alpha_j \leqslant 0, \end{cases} \quad \text{(A3)}$$

where α_j is the angle between the the grid j and the grid jm, and $\alpha_j = 2\pi(j - jm)/l$ (with jm indicating the grid where maximum value occurs, and l as a function of the width of the energy spectrum). If the action spectrum $A_j^{(n+m)}$ has more than one maximum, we should define $jm_1, jm_2, \ldots$ and $l_1, l_2, \ldots$ corresponding to each local action maximum. Combining Eq. (A3) with (A2), we have

$$rr^{(n+m)} \sum_{j=1}^{L} \log_{10}(\cos^2\alpha_j) = \sum_{j=1}^{L} \log_{10} A_j^{(n)} - \log_{10}[A_j^{(n+m)} - FF_j^{(n+m/2)}\Delta t]; \quad \text{(A4)}$$

consequently,

$$rr^{(n+m)} = \frac{\sum_{j=1}^{L} \log_{10} A_j^{(n)} - \sum_{j=1}^{L} \log_{10}[A_j^{(n+m)} - FF_j^{(n+m/2)}\Delta t]}{\sum_{j=1}^{L} \log_{10}\cos^2\alpha_j}. \quad \text{(A5)}$$

The accuracy of the energy conservation can be defined as high as one wants. This filter is very effective for the second-order semi-implicit scheme, which was introduced in the section 2a(2). With this filter, the numerical scheme is computationally stable, and the dispersion effects are largely eliminated. This filter can produce reasonable numerical solutions as shown in Figs. 4 and 7b.

REFERENCES

Book, D. L., and S. T. Zalesak, 1981: Flux-corrected transport. *Finite-Difference Techniques for Vectorized Fluid Dynamics,* D. L. Book, Ed., Springer Verlag, 29–55.

——, J. P. Boris, and K. Hain, 1975: Flux-corrected transport. II: Generalization of the method. *J. Comput. Phys.,* **18,** 248–283.

Boris, J. P., and D. L. Book, 1973: Flux-corrected transport. I: SHASTA, a fluid transport algorithm that works. *J. Comput. Phys.,* **11,** 38–69.

——, and ——, 1975: Solution of the continuity equation by the method of flux corrected transport. *Methods Comput. Phys.,* **16,** 85–129.

——, and ——, 1976: Flux-corrected transport. Part III: Minimal error FCT algorithms. *J. Comput. Phys.,* **20,** 397–431.

Chen, H. S., 1992: Taylor–Galerkin method for wind wave propagation. *Proc. Ninth Conf. Engineering Mechanics,* ASCE, 87–90.

Gelci, R., H. Cazalé, and J. Vassal, 1957: Prévision de la houle. La méthode des densités spectroangulaires. *Bull. Inf. Comité Central Oceanogr. Etude Côtes,* **9,** 416–435.

Günther, H., Hasselmann, S., and P. A. E. M. Janssen, 1993: The WAM model cycle 4. DKRZ WAM Model Documentation, 91 pp.

Kriess, H. O., and J. Lorenz, 1990: *Initial Boundary Value Problems and Navier–Stokes Equation,* Cambridge Press.

Lin, R.-Q., R.-X. Huang, and J. Apel, 1992: A study of the astronomical theory of ice ages in a two-dimensional nonlinear climate model. *J. Geophys. Res.,* **97**(D9), 10 029–10 036.

Phillips, N. A., 1959: An example of non-linear computational instability. *Atmosphere and Sea in Motion. Rossby Memorial Vol.,* B. Bolin, Ed., Rockefeller Institute Press, 501 pp.

Phillips, O. M., 1977: *The Dynamics of the Upper Ocean.* 2d ed. Cambridge Press, 336 pp.

Press, W. H., B. P. Flannery, S. A. Teukolsky, and W. T. Vettering, 1988: *Numerical Recipes in C: The Art of Scientific Computing.* Cambridge Press.

Reider, K. F., J. A. Smith, and R. A. Weller, 1994: Observed directional characteristics of wind, wind stress, and surface waves on open ocean. *J. Geophys. Res.,* **99,** 22 575–22 589.

Shu, C. W., and S. Osher, 1989: Efficient implementation of essentially non-oscillatory shock-capturing scheme. Part II: *J. Comput. Phys.,* **83,** 32–78.

SWAMP Group, 1985: *Ocean Wave Modelling.* Plenum Press, 256 pp.

SWIM Group, 1985: A shallow water intercomparison of three numerical wave prediction model (SWIM). *Quart. J. Meteor. Soc.,* **111,** 1087–1112.

Tolman, H. L., 1992a: A third-generation model for wind waves on slowly varying, unsteady, and inhomogeneous depth and currents. *J. Phys. Oceanogr.,* **21,** 782–797.

——, 1992b: Effects of numerics on the physics in a third-generation wind-wave model. *J. Phys. Oceanogr.,* **22,** 1095–1111.

The WAMDI Group, 1988: The WAR model—a third generation ocean wave prediction model. *J. Phys. Oceanogr.,* **18,** 1775–1810.